NTNU – Trondheim
Norwegian University of
Science and Technology

Nanoparticle effect on Interfacial Properties related to Enhanced Oil Recovery

Line Andreassen

Petroleum Geoscience and Engineering
Submission date: April 2015
Supervisor: Ole Torsæter, IPT

Norwegian University of Science and Technology
Department of Petroleum Engineering and Applied Geophysics

Introduction

We have reached a point in petroleum engineering where the oil production we get from primary and secondary recovery isn't enough anymore. Enhanced oil recovery (EOR) techniques are going to be important in almost every oil field in the coming years. To this end, more and more research is done to find new EOR techniques. The use of nanoparticles as an EOR technique is still new, but shows great promise.

This master thesis focuses on the influence of nanoparticles on fluid properties, mainly interfacial tension and wettability. The nanoparticles used are a new type of nanoparticles, Funzionano, developed by SINTEF Materials and Chemistry.

The nanoparticles are dissolved in synthetic seawater, and two nanoparticle concentrations are used in the measurements. Five crude oils from Norwegian fields are used with the nanofluids.

The focus of the experimental part of the thesis is the interfacial tension and contact angle measurements, which are performed using an SVT 20 spinning drop video tensiometer for interfacial tension and a CAM 200 optical surface tension/contact angle meter for contact angle.

Abstract

Enhanced oil recovery is becoming more important for oil production every year, and the use of nanoparticles is a very exciting new branch of enhanced oil recovery that has many applications.

This thesis takes a look at what has been done before, and then experimentally investigates the effect of nanoparticles on fluid properties, in particular interfacial tension and wettability. The nanoparticles used are a new type of nanoparticles, Funzionano, developed by SINTEF Materials and Chemistry.

Measurements were performed using nanofluids with two different nanoparticle concentrations, 0.5weight% and 1.0weight%, and with 5 different crude oils from Norwegian oil fields.

The interfacial tension was measured using an SVT 20 spinning drop video tensiometer, and the contact angle was measured using a CAM 200 optical surface tension/contact angle meter.

Results from the experiments show that addition of nanoparticles to synthetic seawater reduces both interfacial tension and contact angle, yielding the best results when using the 0.5weight% nanofluid.

While there is a reduction in interfacial tension from the addition of nanoparticles, it is not enough to expect a significant change in oil recovery because of it. That being said, the results are promising and more experiments with for example different nanoparticle concentrations may yield better results.

Sammendrag

Enhanced oil recovery (EOR, avanserte utvinningsmetoder) blir mer og mer viktig for oljeproduksjonen hvert år, og bruk av nanopartikler er en spennende ny gren innenfor EOR som har mange mulige nytteområder.

Denne oppgaven ser på hva som har blitt gjort før, og utforsker så eksperimentelt effekten av nanopartikler på fluidegenskaper, spesielt med tanke på grenseflatespenning og fuktegenskaper. Nanopartiklene som blir brukt er en ny type nanopartikler, Funzionano, som er utviklet av SINTEF Materialer og Kjemi.

Målinger ble utført med nanofluider med to forskjellige nanopartikkelkonsentrasjoner, 0.5vekt% og 1.0vekt%, og med 5 forskjellige råoljer fra norske oljefelt.

Grenseflatespenningen ble målt med et "SVT 20 spinning drop video tensiometer", og kontaktvinkelen med et "CAM 200 optical surface tension/contact angle meter".

Resultatene fra eksperimentene viser at å tilføre nanopartikler til syntetisk sjøvann reduserer både grenseflatespenning og kontaktvinkel, med best resultat fra nanofluiden med 0.5vekt% nanopartikler.

Selv om det ses en reduksjon i grenseflatespenningen ved å tilfør nanopartikler, er det ikke nok til å forvente en betydelig endring i utvinningsgraden på grunn av denne endringen. Til tross for dette er resultatene lovende, og påfølgende eksperiment med for eksempel andre nanopartikkelkonsentrasjoner vil kanskje gi bedre resultater.

Acknowledgements

I owe a big thank you to the SINTEF employees working on the SIP-SURFLUX project, who was very welcoming, and in particular to Umer Farooq, Juan Yang and Nicolas Rival, who have always provided help when needed. Also to Katherine Aurand, who was very patient with me in the lab whenever I needed help, and to Professor Ole Torsæter who always stayed positive, even when I did not.

Contents

List of Figures

List of Tables

1. Theory

1.1 Enhanced Oil Recovery

1.1.1 What is enhanced oil recovery?

Back in the day when the oil production first started there was one main mechanism that made it possible to get the oil up from under the ground, the pressure differential. Higher pressure in the reservoir than in the wellbore pushed the oil into the well and up. This, and the use of pumps, is the basis of what we call primary recovery. But as oil is produced, the pressure in the reservoir decreases. When the pressure reaches bubble point pressure, gas will start to come out of solution. This can help maintain pressure so we produce oil longer, but it can also result in gas being produced instead of oil. Such intrusion of gas, and also water, to the production well reduces oil production severely and it may no longer be economical to keep producing from a well after gas or water breakthrough. So when this happens, or when the pressure in the reservoir is simply too low to yield much production, production through only primary production is over.

This doesn't mean there is no more oil in the reservoir, so developing ways to maintain the pressure so that it stays above the bubble pressure became the next step. This can be achieved by drilling another well and injecting water or gas, and goes under the term secondary production. This leads to more of the oil in the reservoir being produced before production is no longer economical.

Again, this doesn't mean there is no more oil in the reservoir. So reservoir engineers started devising even more advanced ways to get more. This includes chemical methods, thermal methods and other injection than just water or standard gas. This is called tertiary recovery.

The terms tertiary recovery and enhanced oil recovery (EOR) is often used interchangeably, but some consider EOR to be any method more advanced than those described as primary and secondary recovery that is used at any point in the life of the field, not only at the tertiary stage.

1.1.2 Some current enhanced oil recovery techniques

Chemical processes

There are three main chemical processes used for EOR today; surfactant flooding, alkaline flooding and polymer flooding. In these processes chemicals are added to the water used for waterflooding, changing its purposes in various ways.

Surfactant flooding is performed by adding surface acting agents to the water. This is done mainly to reduce surface and interfacial tension. These are organic compounds composed of a hydrophobic hydrocarbon chain called the "tail", and a polar hydrophilic group called the "head". Due to their composition such compounds are soluble in both water and organic solvents. They adsorb on surfaces or interfaces, thus altering surface or interfacial properties. Their main use is that they reduce surface and interfacial tension [Sheng, 2011, chap. 7].

Alkaline flooding is performed by adding alkali to the water. The most commonly used alkali for this purpose are sodium hydroxide and sodium carbonate, but other used alkali are soduim orthosilicate, sodium tripolyphosphate, sodium metaborate, ammonium hydroxide and ammonuim carbonate. These alkali react with organic acids in crude oil in the reservoir and produce in situ surfactants that are capable of lowering interfacial tension. Adding the alkali increases pH, which in turn lowers surfactant adsorpsion, so that a smaller surfactant concentration is needed. Alkaline flooding is also called caustic flooding [Sheng, 2011, chap. 10].

Polymer flooding improves waterflooding by altering the mobility ratio, which is the ratio of displacing fluid mobility to displaced fluid mobility [Sheng, 2011, chap. 4].

$$M = \frac{k_{rw}}{k_{ro}} \frac{\mu_o}{\mu_w} \tag{1.1}$$

A mobility ratio less than 1 is favorable [Torsæter, 2011b]. Lowering the mobility ratio can either be obtained by lowering oil viscosity or by increasing water viscosity. Decreasing oil viscosity is often not a realistic goal without adding heat, so polymers are added to the waterflood to increase water viscosity.

The two main types of polymers are hydrolyzed polyacrylamide (HPAM) and xanthan gum. HPAM is a synthetic polymer while xanthan is a biopolymer [Sheng, 2011, chap. 5].

Thermal processes

Steam injection, or steam flooding, is the process of injecting steam generated at the surface to heat up crude oil and reduce its viscosity. In addition to reducing oil viscosity the steam flood also contributes to oil production by partly condensing and generating an artificial drive that sweeps oil towards the producing wells ["Steamflood"].

In-situ combustion, or fire-flooding, works by burning off a portion of the resident oil. To do this, an oxidizing gas, air or oxygen-enriched air, is injected and ignited. Oil is driven towards the producing well by a combination of water-, steam- and gasdrive ["In-situ combustion"].

Carbon dioxide flooding

CO_2 flooding is based on injecting CO_2 into the reservoir after regular waterflooding is finished. The CO_2 mixes with the formation oil and the resulting fluid has low viscosity and low surface tension, making it easier to displace the oil. CO_2 may also invade zones or pores that could not be invaded during waterflood and release trapped oil ["API Background Report"].

1.2 Fluid properties

1.2.1 Density

Density is a measure of mass per volume unit, and can be easily calculated using the following equation:

$$\rho = \frac{m}{V} \tag{1.2}$$

where ρ is density, m is mass and V is volume. The SI unit for density is kg/m^3, and other often used units include g/cm^3, g/ml and lb/ft^3.

Other properties closely related to density include specific weight, defined as weight per volume (N/m^3), and specific gravity, being the ratio of the density of a substance to the density of water (unitless) ["Density, Specific Weight and Specific Gravity"].

1.2.2 Viscosity

Viscosity is a measure of a fluids resistance to flow. The easier a liquid flows, the less viscous it is. We separate between dynamic and kinematic viscosity.

The dynamic viscosity of a liquid is a measure of its inner resistance to movement. Newton's law of friction defines the shear stress between layers of a non-turbulent, Newtonian fluid:

$$\tau = \mu \frac{dc}{dy} \tag{1.3}$$

where

τ = shear stress
μ = dynamic viscosity
dc = liquid velocity
dy = distance between layers

The SI unit of viscosity is Pascal seconds (Pa s), but more widely used are poise (p), centiPoise (cP) and dyne s/cm^2, where

1 Pa s = 10 dyne s/cm^2 = 10 p = 1000 cP

The kinematic viscosity is the ratio between the dynamic viscosity and the density, and can be calculated thus:

$$\nu = \frac{\mu}{\rho} \tag{1.4}$$

where ν = kinematic viscosity.

Using kinematic viscosity eliminates force from calculations, and is represented by the SI unit m^2/s, Stoke (St) or centiStoke (cSt), where

1 St = 10^{-4} m^2/s = 1 cm^2/s
1 cSt = 0.01 St = 10^{-6} m^2/s = 1 mm^2/s

["Dynamic, Absolute and Kinematic Viscosity"]

1.2.3 Surface and interfacial tension

Surface tension (γ) is defined as the work required to increase the area of a surface isothermally by a unit amount.

This work is carried out by short-range intermolecular forces working on the interface between two phases (gas-liquid or liquid-liquid). These forces comprise mainly London dispersion forces, but also other forces such as hydrogen bonds (like in water), metal bonds (like in mercury) and polar forces. For hydrocarbons no other forces than the dispersion forces affect surface tension.
Surface and interfacial tensions are essentially the same, but the terms are used differently. Surface tension is used when one of the phases is gaseous, and interfacial tension is used when both phases are non-gaseous.

Consider a water-oil interface. The molecules in the water are attracted towards the water phase by interactions within the water phase (dispersion forces and hydrogen bonds), and attracted towards the oil phase by interactions between oil and water (dispersion forces only). In the same way the molecules in the oil are attracted towards the oil phase by interactions within the oil phase (dispersion and other), and attracted towards the water phase by interactions between the two phases (dispersion forces only).
The interactions between oil and water are often decided by taking the geometric mean of the dispersion forces inside the water phase and the oil phase.

We then have

Forces inside the water: $\gamma_1 = \gamma_1^d + \gamma_1^h$
Forces inside the oil: $\gamma_2 = \gamma_2^d$
The oil-water interactions: $(\gamma_1^d \gamma_2^d)^{1/2}$

where the superscripts d and h denote dispersion forces and hydrogen bond forces, and the subscripts are 1 for water and 2 for oil.

Combining these we get:

Tension on the water molecules at the interface: $\gamma_1 - (\gamma_1^d \gamma_2^d)^{1/2}$
Tension on the oil molecules at the interface: $\gamma_2 - (\gamma_1^d \gamma_2^d)^{1/2}$

This leads to an equation for total tension on the interface first formulated by Fowkes:

$$\gamma_{12} = \gamma_1 + \gamma_2 - 2(\gamma_1^d \gamma_2^d)^{1/2} \tag{1.5}$$

This equation has shown to only be valid when we assume that the only interaction between the two phases are the dispersion forces [Shaw, 1992, pp. 64-67].

The SI unit of surface and interfacial tension is N/m, but mN/m is more often used, as this is more convenient.

As mentioned, for Fowkes' equation to be applicable we have to exclude all interaction between the phases except dispersion forces. Wu [1971] developed an equation that takes polar forces into account. He uses ϕ^d and ϕ^P to denote the total interaction between phases for dispersion and polar forces, respectively.

The interfacial tension can then be written as:

$$\gamma_{12} = \gamma_1 + \gamma_2 - 2\phi^d - 2\phi^p \tag{1.6}$$

In Fowkes' equation the dispersion term is approximated by using the geometrical mean. This hints that doing the same for the polarity term is a good idea. Unfortunately, this has been seen not to be the best solution, and instead Wu proposes using what they call the "reciprocal" mean, which is better known as the harmonic mean. Then we get

$$\phi^d = \frac{2\gamma_1^d \gamma_2^d}{\gamma_1^d + \gamma_2^d} \tag{1.7}$$

$$\phi^P = \frac{2\gamma_1^P \gamma_2^P}{\gamma_1^P + \gamma_2^P} \tag{1.8}$$

Using the harmonic mean in the equation for interfacial tension this gives

$$\gamma_{12} = \gamma_1 + \gamma_2 - 4\left(\frac{\gamma_1^d \gamma_2^d}{\gamma_1^d + \gamma_2^d}\right) - 4\left(\frac{\gamma_1^P \gamma_2^P}{\gamma_1^P + \gamma_2^P}\right) \tag{1.9}$$

One case where considering polar forces is important is when working with polymer systems.

1.2.4 Wettability and contact angles

Wettability is the preference of a solid to be in contact with one fluid rather than another. The preferred fluid is called the wetting fluid, and it will displace a non-wetting fluid. At the extremes the wetting fluid will spread out completely on a solid surface to maximize contact while the non-wetting fluid will minimize contact and try to create a spherical bead. The conditions in between these extremes are described by the use of the contact angle.

The contact angle describes the relation between the interfacial tensions working in the system. For a system with a solid, water and an oil drop, we have

$$\gamma_{so} = \gamma_{sw} + \gamma_{ow} \cos\phi \tag{1.10}$$

where the subscripts so, sw and ow denote the solid-oil interface, the solid-water interface and the oil-water interface, and ϕ is the contact angle, as shown in figure 1.1.

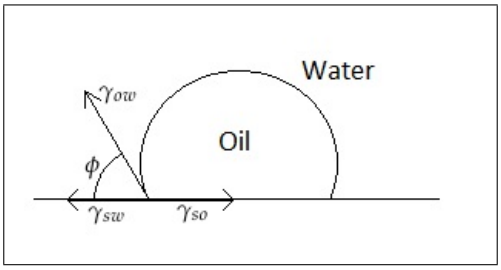

Figure 1.1: Contact angle for an oil drop in water

For a case where the oil creates a drop approaching spherical form we have what we call a water-wet surface. Conversely, if the oil drop spreads out we have an oil-wet surface. For the cases in the middle the surface has little or no preference and we call that neutral-wet or intermediate-wet [Abdallah et al., 2007].

Which side of the oil-water interface the contact angle is measured on varies in literature, but the convention is to measure on the side of the denser phase [Blunt, 2001]. In most oil-water systems this will be the water, so for a water-wet surface the contact angle approaches 0° and for an oil-wet surface the contact angle approaches 180°. If the opposite angle is given, it is easily adjusted to follow convention by subtracting the angle from 180°, in accordance with equation 1.11.

$$\phi_{\text{denser phase}} + \phi_{\text{less dense phase}} = 180^\circ \tag{1.11}$$

In a reservoir we may encounter any of these wetting conditions, and not necessarily a consistent one. The specifics of the reservoir rock will vary, and changes in oil and water saturation in different parts of the reservoir could lead to there being different wetting conditions throughout the reservoir. Such reservoirs are characterized as mixed-wet.

1.3 Relative permeability and capillary pressure

Absolute permeability is a measure of a fluids capacity for flow through porous media. It is defined by Darcy's Law [”Relative permeability and capillary pressure”, 2013]:

$$q = -\frac{kA}{\mu}\frac{\Delta P}{L} \tag{1.12}$$

where

q	=	flow rate
k	=	absolute permeability
A	=	cross-sectional flow area
μ	=	viscosity
ΔP	=	pressure drop
L	=	length

When we have more than one phase, we need a separate equation for each phase. To this end, the effective permeability is introduced. k_w and k_o is the effective permeability of water and oil, respectively, and is a measure of each fluids ability to flow when it doesn't occupy 100% of the pore space.

For a system with oil and water we will have the following equations for flow in the x-direction

$$q_w = -\frac{kk_{rw}A}{\mu_w}\frac{\delta p_w}{\delta x} \tag{1.13}$$

$$q_o = -\frac{kk_{ro}A}{\mu_o}\frac{\delta p_o}{\delta x} \tag{1.14}$$

and similar equations for flow in y and z directions.

The k_{rw} and k_{ro} terms are called relative permeabilities and is the ratio between effective permeability and the absolute permeability.

$$k_{ro} = \frac{k_o}{k}$$

$$k_{rw} = \frac{k_w}{k}$$

The relative permeabilities are often represented as a function of saturation in a graph, like in figure 1.2, and by studying the relative permeability curves for oil and water we can learn much about the flow of fluids in a reservoir.

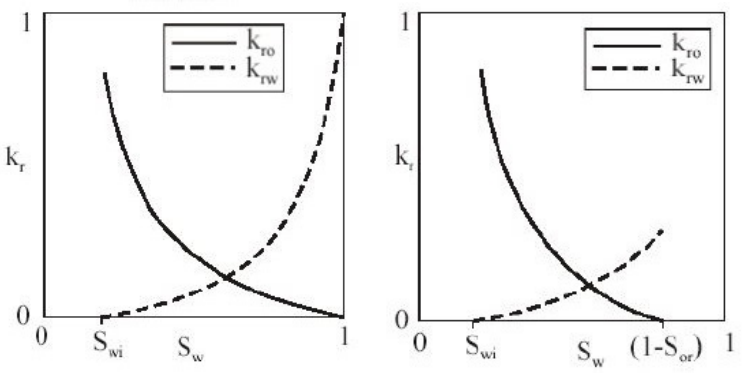

(a) Drainage (b) Imbibition

Figure 1.2: Relative permeability curves [Torsæter, 2011b]

The relative permeability graphs act different depending on whether water saturation is increasing or decreasing, which is what the drainage and imbibition terms in figures 1.2a and 1.2b refer to. When the saturation of the wetting phase is decreasing the process is called drainage, and when the saturation of the wetting phase is increasing it is called imbibition. Often in reservoir engineering the term drainage is used for when the water phase is decreasing regardless of wetting preferences [Torsæter, 2011b].

Capillary pressure is the difference in pressure across an interface separating two immiscible fluids, and is defined as the pressure of the non-wetting phase minus the pressure of the wetting phase. As with the relative permeabilities the actual wetting preferences are often disregarded, and capillary pressure is often defined as the pressure of oil minus the pressure of water. The capillary pressure can be represented by a graph such as the one in figure 1.3 [Torsæter, 2011a].

1.4 Influence of fluid properties

1.4.1 Interfacial tension

A study was done by Amaefule and Handy [1982], looking at Berea sandstone cores, initially saturated with 1% brine and interfacial tension ranging from 34 mN/m to 0.01 mN/m. In this study several changes to the relative permeability curves were recorded. Decreasing the interfacial tension of the waterflood showed an increase in both oil and water relative permeability at S_w. Such an increase leads to the curves becoming "less curved" and as interfacial tension approaches zero they will approach a linear slope. In addition to this, the endpoint residual

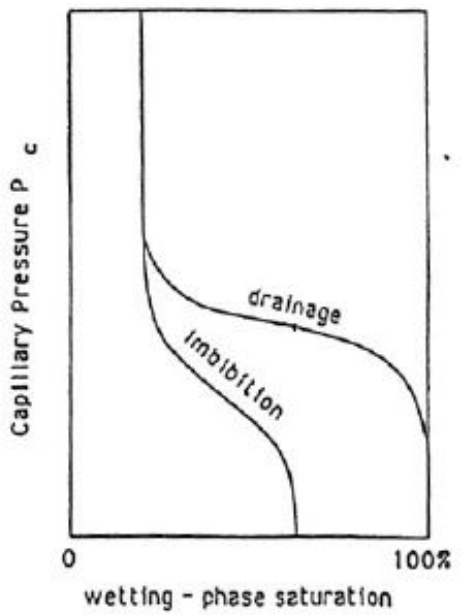

Figure 1.3: Capillary pressure [Torsæter, 2011a]

saturations for both water and oil (S_{wir} and S_{or}) decrease, which has an effect on the amount of recoverable oil, and the difference in the curves between drainage and imbibition (hysteresis) diminishes. There is also seen a difference in how a change in interfacial tension affects relative permeabilities depending on whether we are looking at steady or unsteady state data. Steady state results show better predictions for oil recovery than unsteady state results. For unsteady state there is only seen a difference in k_{ro} at low oil saturation, while a difference in k_{rw} is seen for all saturation values. Both steady and unsteady state data indicate less water-wet rock surfaces when decreasing IFT. Amaefule and Handy observed no changes for IFT values higher than 0.1 mN/m, but Leverett [1939] showed a small but definite increase in both oil and water relative permeabilities when reducing interfacial tension from 24 mN/m to 5 mN/m.

Longeron [1980] did tests on Fountainebleau sandstone displacing oil with gas with a filtration velocity of about 20 cm/hr. Results from these test show major change in relative permeability when the interfacial tension is reduced to around 0.04 mN/m. Numerical simulations for values of 0.001 mN/m shows the relative permeability curves represented as two lines with a linear slope in the relative permeability - saturation diagram. In addition to the changes seen in the relative permeability diagrams, it is also observed that recovery at vapor breakthrough becomes greater as the interfacial properties of vapor and liquid come closer together.

Reducing interfacial tension will make it easier for oil droplets to move through

pore throats by reducing work of deformation needed. Lowering interfacial tension increases the capillary number. A higher capillary number results in an increase in oil displacement efficiency [Donaldson et al., 1989, chap. 10].

Donaldson et al. claims the interfacial tension must be lowered to the range of 0.01 to 0.1 mN/m for it to be possible to displace residual oil, a view that is supported by Wagner and Leach [1966] who estimate that a value less than 0.07 mN/m is needed to achieve increased recovery at the time of breakthrough in their specific system.

1.4.2 Wettability

Owens and Archer [1971] performed tests on samples of Torpedo outcrop sandstone, and reported that increasing the contact angle (reducing water-wetness) lowered relative permeability to oil, and increased relative permeability to water. Also, the crossing point between the oil and water relative permeability curves moved to the left and down with increased contact angle.

Abdallah et al. [2007] show that the endpoint relative permeability of water at 1-S_{or} is lower for water-wet than for mixed-wet, while endpoint relative permeability of oil at S_{wir} is higher for water-wet than for mixed-wet.

The different wetting conditions have different effects in a reservoir. In a water-wet reservoir a situation may arise where oil is being trapped in pores where the capillary pressure is not high enough for the water to enter the pores. In an oil-wet reservoir there will be a thin layer of oil closest to the rock surface so the oil has a continuous path where it can leave such pores where the oil would be trapped in a water-wet reservoir. On the other hand, in an oil-wet reservoir a certain amount of oil is held back in the reservoir, sticking to the rock surface, which can't be produced. In water-wet reservoirs water breakthrough will occur later in a waterflood and more oil will be produced before breakthrough, compared to an oil-wet reservoir. In addition to this, simulations have shown more oil recovery from water-wet layers than oil-wet layers when other conditions are similar [Abdallah et al., 2007].

1.4.3 Relative permeability

As mentioned before, relative permeability curves can provide good insight to the flow conditions in a reservoir, and a few specific points are important to consider.

End point saturations, the irreducible water saturation (S_{wir}) and the residual oil saturation (S_{or}), indicate the amount of water or oil that can't be removed from the rock at current conditions. They determine the movable saturation range and are directly related to the amount of recoverable oil. End point relative permeabilities, k_{rw} at S_w = 1-S_{or} and k_{ro} at S_w = S_{wir}, show the relative permeability of a phase where that phase occupies as much as the pore space as possible. It is used to

determine the mobility ratio, which is an important parameter in determining sweep efficiency in a displacement process.

In addition to this the shape of the curves may give info on recovery efficiency, and the point where the relative permeability curves cross gives an indication of the wetting preferences of the rock [Torsæter, 2011a].

1.5 Nanoparticles

Nanoparticles are defined as any particle with dimensions in the 1 - 100 nanometers (1 nm = $1 \cdot 10^{-9}$ m) range [IUPAC, 2012]. It has been discovered that properties of many materials tend to change significantly as we enter nanoscale. On this scale quantum effects will dominate, and many properties (melting point, chemical reactivity, fluorescence etc.) will change with changing particle size ["What's So Special about the Nanoscale?"].

The suspension of nanoparticles in a fluid is called a nanofluid. Nanotechnology is a term that can be applied broadly, simply being technology that utilizes nanoparticles, and is investigated in many fields. Medicine, biotechnology, energy applications, water treatment and petroleum production are some of many, and all of these have many subcategories as well.

Nanoparticles can be used for many things, among them material design, electronics, biomedicine and enhanced oil recovery. Several types of nanoparticles are in use today. Liposomes, which are used in biomedicine for drug delivery by encapsulating the drug in liposome nanoparticles. Carbon nano tubes, which are cylinders formed of graphite sheets. These are mechanically very strong and has semiconductor properties. Quantum dots, which are particles where adsorpsion and emmision are controlled by particle size. These are used among other things as contrast agents for flourescence microscopy. There are also magnetic nanoparticles and metallic nanoparticles [Bennetzen and Mogensen, 2014].

1.5.1 Nanoparticles in the oil industry

Nanoparticle uses in the oil industry include using sensors designed to respond to changes in pressure, temperature, shear rate, salinity and other specifics for reservoir characterization. The same reservoir conditions can be used to release encapsulated chemicals in specific regions of a reservoir, or after a certain amount of time. Removal of specific ions from aqueous solutions, and removal of oil from water-oil emulsions, which can be important in treating production water, are also a possibility [Bennetzen and Mogensen, 2014].

Using nanoparticles to decrease water invasion in shale formations

In shale formations a problem often arises because the fluids in a water based mud can't be stopped from penetrating the wellbore. The shale has nanosized pores that particles in the drilling fluid are not able to seal, and an effective mudcake will not be built on the shale surface. This results in swelling of the wellbore and can lead to wellbore instability [Cai et al., 2012].

Nanotechnology offers a solution to this. Cai et al. [2012] did experiments on Atoka shale that show that adding nanoparticles to the drilling fluid can reduce

permeability in the shale, with the most effective nanoparticles having a size between 7-15 nm. Tests with nanoparticles over 20 nm were also performed, but showed poorer results, possibly due to the inability of these particles to enter the pores. They used a nanoparticle concentration of 10wt.%.

[Sensoy et al., 2009] also performed measurements on Atoka shale and also obtained good results by adding nanoparticles to drilling fluids, but had better results with 20 nm sized nanoparticles than with 5 nm sized nanoparticles. They also achieved reduction in fluid penetration in Gulf of Mexico shale, though the results here were not quite as good. This study shows that using less than 10wt.% nanoparticles is not as effective.

Using nanoparticles to control fines migration

Fines migration is a term used for the movement of small (usually smaller than 37 micrometers) solid particles in the pores of sandstone reservoirs. These small particles tend to move with the reservoir fluids toward the production well and are often redeposited near the wellbore. This can cause problems such as localized plugging and areas of extra high fluid velocity, which may cause erosion and failure in sand screens [Huang et al., 2008].

To combat this, Huang et al. [2008] tested the possibility of attaching nanoparticles to proppant packs so that the formation fines would be attracted to the nanoparticles and thus kept from moving towards the wellbore. They showed in laboratory tests that treating proppant packs and sand packs with nanoparticles had the wanted effect and that the formation fines were held back by the nanoparticles.

1.5.2 Nanoparticles in enhanced oil recovery

Nanoparticles are ideal in harsh environments such as reservoirs due to their mechanical and thermal stability. There is research supporting their use in EOR for wettability alteration, stabilization of foam or emulsions, conformance control, viscosity modification, interfacial tension reduction and reduction of residual oil saturation, all of which can improve oil recovery.

Ogolo et al. [2012] looked into the use of several different types of nanoparticles they thought likely to be used in reservoir engineering. They used oxides of aluminium, zinc, magnesium, iron, zirconium, nickel, tin and silicon to investigate EOR possibilities by performing experiments under surface conditions. Distilled water, brine, ethanol and diesel were used as dispersion media for the nanoparticles.

The main knowledge from this investigation is that aluminium oxide in brine and distilled water seem to reduce the viscosity of oil and that silicon oxide has significant effect on wettability, both resulting in improved oil recovery. Nickel and iron oxide also give good results, while magnesium and zinc oxide caused permeability problems.

Nanoparticle effect on wettability and interfacial tension

One of the main aims for nanoparticles in enhanced oil recovery is the alteration of interfacial tension and wettability.

Li et al. [2013] performed experiments utilizing hydrophilic silica nanoparticles with an average particle size of 7 nm along with a light crude oil from the North Sea. They performed interfacial tension and contact angle measurements as well as flooding on two types of porous media; a glass micromodel and berea sandstone cores.

Their results show a reduction of interfacial tension from 19.2 mN/m with brine to approximately 11 mN/m and 8 mN/m for 0.01wt.% and 0.05wt.% respectively. They also show a reduction of contact angle from 54° with brine to 40° with 0.01wt.%, 31° with 0.05wt.% and 22° with 0.10wt.%, which means slightly increased water-wetness with added nanoparticles.

Roustaei et al. [2012] performed similar interfacial tension, contact angle and core flooding experiments. They used two types of polysilicon nanoparticles, hydrophobic and lipophilic polysilicon (HLP) and naturally wet polysilicon (NWP) along with a degassed oil from an Iranian reservoir. The core flooding was performed on sandstone rocks, also from an Iranian reservoir.

Like Li et al. their results showed a reduction in interfacial tension, from 26.3 mN/m to 1.75 mN/m and 2.55 mN/m for HLP and NWP respectively. The contact angle results on the other hand show results opposite of Li et al., with a clear change from water-wet to neutral-wet for both HLP and NWP.

Both of these studies also showed significantly improved oil production from core flooding when the core was flooded with nanofluid after regular waterflooding.

Karimi et al. [2012] investigated the effects on wettability alteration in carbonate reservoirs, using ZrO_2 nanoparticles. In originally oil-wet rock from a reservoir near the Nowroox field, with a crude oil from the Newrooz field, experiments showed that the wettability changed from strongly oil-wet to strongly water-wet.

Using nanoparticles to improve CO_2 injection

One popular EOR method is CO_2 injection. This is an effective method in many cases, but has some problems, especially in thick reservoirs, since CO_2 has a relatively low density and viscosity.

In reservoirs where the resident fluids have higher density than CO_2, the injected CO_2 tends to bypass oil by floating to the top of the reservoir. Especially in thick reservoirs this can lead to quite a lot of oil being bypassed. Similarly, the low viscosity of the CO_2 can lead to viscous fingering causing early CO_2 breakthrough, poor sweep efficiency, increased amount of CO_2 used and lower oil recovery.

Similar problems also occur in fractured reservoirs and very heterogeneous reservoirs where the CO_2 is quick to enter high permeability sections, thus bypassing

oil in the lower permeability sections. This problem is somewhat tackled using the water-alternating-gas process, but its effectiveness is reduced when moving further away from the wellbore.

Due to these issues, reservoir engineers are looking into using CO_2-foams to increase the viscosity of the CO_2. Such foams can be generated using water- or CO_2-soluble surfactants or nanoparticles.

The reasoning for using nanoparticles is that surfactant-stabilized foams have some issues with stability under reservoir conditions, while studies have shown that small solid particles such as fumed silica can stabilize drops in emulsions and bubbles in foam by adsorbing at fluid/fluid interfaces.

Al Otaibi et al. [2013] performed experiments that resulted in stable water/iso-octane emulsions that gelled with time. They were generated at different water/iso-octane volume percentages and different nanoparticle concentrations, and changing these properties altered the stability of the foam. They also achieved stable CO_2/water and water/CO_2 emulsions, where the CO_2/water emulsions greatly enhanced the viscosity of liquid CO_2.

1.5.3 Nanoparticle theories

Understanding of why nanoparticles has such an effect is still not complete. To describe interactions between nanoparticles, fluids and rock surfaces, DLVO theory and Poisson-Boltzmann physics are enough for an approximation but for a full understanding many different forces of different origin will have to be taken into account as well.

Particle size

The small particle size results in a very high surface to volume ratio and contact area. This creates a high driving force for diffusion, enhanced mass transfer and can change the properties of a fluid drastically [Ayatollahi and Zerafat, 2012]. Most pore bodies and pore throats can be measured in the microscale [Enbaia and Ramdzani, 2014], meaning that nanosized particles have a very good chance to spread homogenously in porous media, reaching areas of a reservoir that may stay untouched using conventional methods.

Electrical double layer

We consider the reservoir rock to have a charged surface. The gravitational forces working on the nanoparticles are ignored so that the charge forces working are more pronounced. The rock surface is considered to have a constant net charge, and particles in the fluid will arrange in such a way that charges opposite that of the rock surface will be dominating at the interface (positive forces at rock surface, negative forces in fluid at interface). This region ideally consisting of opposite

charges is termed the electrical double layer. This gives us charged nanoparticles and is one of the governing theories trying to predict the interactions between nanoparticles, fluid and rock. The governing equation for the potential at these charged interfaces, which can be used to predict nanoparticle behavior in conjunction with transport equations, is the Poisson-Boltsamn equation [Ayatollahi and Zerafat, 2012].

$$\nabla^2\psi = \frac{2zen_0}{\varepsilon}\sinh(\frac{se\psi}{k_BT}) \tag{1.15}$$

DLVO Theory

DLVO (Derjaguin - Landau - Verwey - Overbeek) theory describes how the stability of two particles in close proximity depends on the total energy of their interactions. It is used to simulate interactions between nanoparticles, between nanoparticles and other particles and between nanoparticles and rock surfaces. DLVO theory takes into account many different interactions, such as the attractive and repulsive forces from electrical double layers, London van der Waals attraction, born repulsion, acid-base interactions and hydrodynamic forces [Ayatollahi and Zerafat, 2012].

1.5.4 Polyhedral Oligomer SilSesquioxsanes

The nanoparticles used in the laboratory part of this thesis were prepared by SINTEF Materials and Chemistry as part of their SURFLUX project, called Funzionano.

The Funzionano nanoparticles belong to a class of nanostructures called Polyhedral Oligomer SilSesquioxsanes (POSS) [Rival, 2015]. These are three-dimensional nanosized building blocks that allow for the creation of hybrid materials with excellent control over properties and nanostructure. They consist of silicon (Si) atoms with connections to three oxygen (O) atoms and with a fourth connection to another molecule, in the case with Funzionano this molecule is NH_2. These atoms are arranged in a cage structure with silicone atoms at the corners, as seen in figure 1.4. The T_8, T_{10} and T_{12} terms refer to the number of Si-atoms in the cage [Markovic et al., 2011].

The Funzionano molecules have an average chemical formula of $SiO_{3/2}$, and the particle size is around 10nm, with an agglomeration of 100nm.

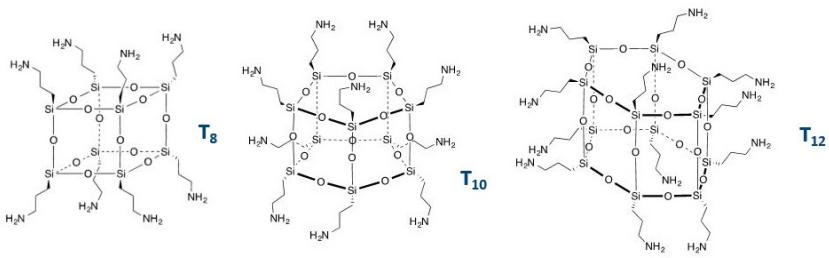

Figure 1.4: Funzionano cage structures [Rival, 2015]

2. Laboratory work

Synthetic seawater was received from Umer Farooq at SINTEF SeaLabs, and used both for direct measurements and for making nanofluids. Table 2.1 shows the recipe used, where the components in red are components that were left out. Which recipe to use was determined by SINTEF with information gained from "Artificial seawater" and Kester et al. [1967].

Table 2.1: Synthetic seawater recipe

Salt	Molecular weight [g/mol]	mol/kg solution	g/kg solution
Gravimetric salts			
Sodium chloride (NaCl)	58.44		23.926
Sodium sulfate (Na_2SO_4)	142.04		4.008
Potassium chloride (KCl)	74.56		0.677
Sodium bicarbonate ($NaHCO_3$)	84.00		0.196
Potassium bromide (KBr)	119.01		0.098
Boric acid (H_3BO_3)	61.83		0.026
Sodium fluoride (NaF)	41.99		0.003
Volumetric salts			
Magnesium chloride ($MgCl_2.6H_2O$)	203.33	0.05327	10.831
Calcium chloride ($CaCl_2.2H_2O$)	147.03	0.01033	1.5188
Strontium chloride ($SrCl_2.6H_2O$)	266.64	0.00009	0.024

2.1 Preparing the nanofluids

A nanofluid sample with a concentration of 92.8wt.% nanoparticles was received from Juan Yang and Nicolas Rival at SINTEF Materials and Chemistry. This sample was diluted to a much smaller concentration with the synthetic seawater blend, where the amount to be added of each component was calculated using equation 2.1

$$m_1 C_1 = m_2 C_2 \tag{2.1}$$

where m is mass, C is concentration and the subscripts 1 and 2 denote the high starting concentration and the low diluted concentration, respectively.

The mass of the highly concentrated nanofluid needed was calculated to fit a volume of finished product. The nanofluid was weighed in a beaker, to a value close to that calculated, and the calculation was redone to fit the mass of seawater to the actual mass of the nanofluid. This was done because it is easier to get an exact number with the seawater as it is less viscous (plus a slight deviation from the optimal values will have less effect on the final concentration if it is in the component with highest added mass, i.e. the water). The mixture was then magnetically stirred before a handheld sonicator was used for 5 minutes to achieve a homogenous blend.

2.2 Density

The liquid density was measured using a standard pycnometer, like the one in figure 2.1.

Figure 2.1: Pycnometer

The volume of the pycnometer is known, and the following procedure gives the weight of the liquid filling that volume.

1. Select a clean, dry pycnometer with stopper
2. Weigh pycnometer (including stopper) when dry

3. Fill pycnometer with the fluid that is being measured and put on stopper, making sure there are no gas bubbles in the liquid, and carefully dry off any liquid residue on the outside of the pycnometer
4. Weigh liquid-filled pycnometer

Equations 2.2 and 2.3 show how the density is found using these measurements.

$$m_l = m_{fp} - m_{dp} \tag{2.2}$$

$$\rho_l = \frac{m_l}{V_l} \tag{2.3}$$

where

m_l	=	mass of liquid being measured
m_{dp}	=	mass of pycnometer when dry
m_{fp}	=	mass of pycnometer when filled
V_l	=	volume of liquid in pycnometer

2.3 Viscosity

The viscosity was measured using a glass capillary viscometer, like the one in figure 2.2. With this method the time it takes for a fixed volume of the liquid to flow through the capillary is measured and used with a calibration constant for that exact viscometer to find the viscosity. With this type of viscometer there is two constants as there are two volumes to measure over, represented by (4) and (6) in figure 2.2.

The following procedure was used to obtain viscosity:

1. Select a clean, dry viscometer
2. Attach a rubber suction ball to tube (1) to be ready to apply suction
3. Turn viscometer upside down and submerge the end of tube (2) in the liquid, and apply suction so that the liquid is sucked into the tube until it reaches mark (8)
4. Turn viscometer the right way up and place it in a stand where it is level. If the liquid is not at room temperature, close the end of tube (1) before the liquid has reached mark (3) and leave it until liquid has reached room temperature
5. Open tube (1) when temperature has been reached and measure the time it takes for the liquid to travel from marks (3) to (5) and from marks (5) to (7).
6. Use these times together with the calibration constant for that exact viscometer to get two calculated viscosities. If the two calculated values are close, the average can be accepted as the correct value, if they are very different the

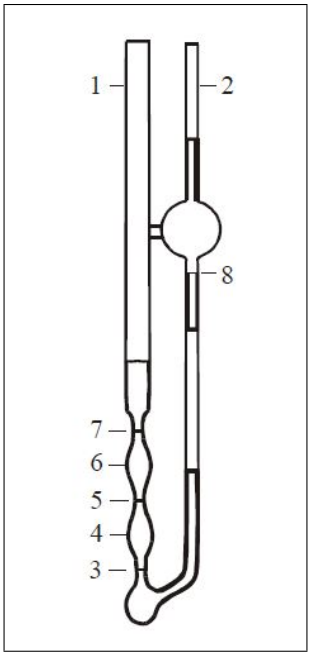

Figure 2.2: Viscometer [Torsæter and Abtahi, 2003]

measurement needs to be redone. Use equation 2.4 for kinematic viscosity or equation 2.5 for dynamic viscosity.

$$\nu = k(t - \vartheta) \tag{2.4}$$

$$\mu = \rho k(t - \vartheta) \tag{2.5}$$

where

ν	=	kinematic viscosity [cSt]
μ	=	dynamic viscosity [cP]
k	=	calibration constant [mm^2/s^2]
t	=	time [s]
ρ	=	density [g/cm^3]
ϑ	=	Hagenbach constant, used if $t < 400s$

2.4 Refractive index

The refractive index was measured using a Mettler Toledo Portable Refractometer. The measurement is very straightforward, one simply fills the glass prism of the device with liquid and pushes the button to calculate.

2.5 Interfacial Tension

The interfacial tension was measured using the Spinning Drop Video Tensiometer SVT 20 apparatus.

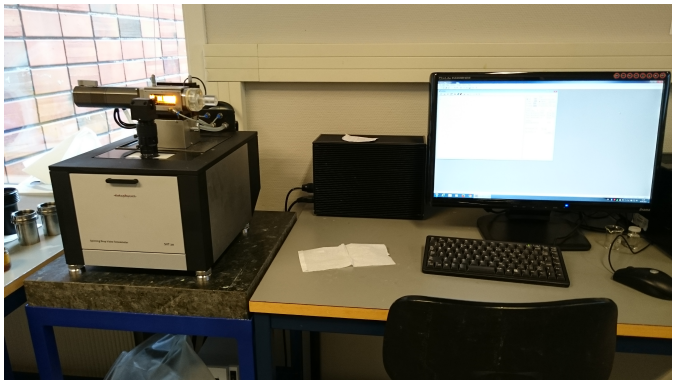

Figure 2.3: Spinning Drop Video Tensiometer SVT 20

The SVT 20 rotates a capillary tube containing two immiscible phases, a single drop of one phase and the other phase filling the rest of the capillary. As the capillary rotates, the rotational force creates separation between the two liquids, with the higher density liquid being pushed away from the center and the lower density liquid forming a drop around the rotational axis. The shape of the drop will depend on the interfacial tension between the liquids, with a low IFT forming a more elongated drop than a high IFT. The drop will also elongate more as the rotational speed is increased [DataPhysics].

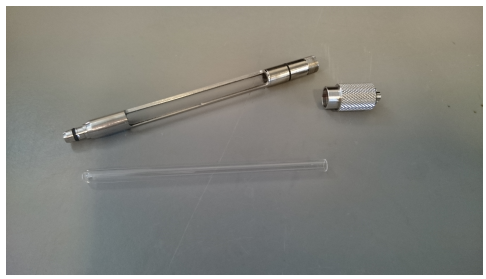

Figure 2.4: Capillary tube and capillary tube holder for SVT 20

The drop inside the capillary gets analyzed by accompanying software and the IFT is calculated using various data, including densities, rotational speed and drop shape. The SVT 20 gives the option of calculating IFT by using algorithms by "Laplace Young", "Cayias, Schechter, Wade" and "Vonnegut" [DataPhysics]. The results given in this paper is calculated with the Laplace Young equation.

Procedure:

1. Select a clean, dry capillary tube of the kind that is made for the SVT 20 equipment
2. Fill capillary with water/nanofluid
3. Use a syringe to inject a drop of oil within the water/nanofluid
4. Place capillary in capillary holder and secure the seal, making sure no air bubbles are in the fluid
5. Place capillary holder in SVT 20 apparatus
6. Start desired rotation
7. Adjust values in the computer program to the correct ones
8. Calibrate the imaging system
9. Start measurement

The IFT measurement is finished when the IFT value has stabilized, like in figure 2.5

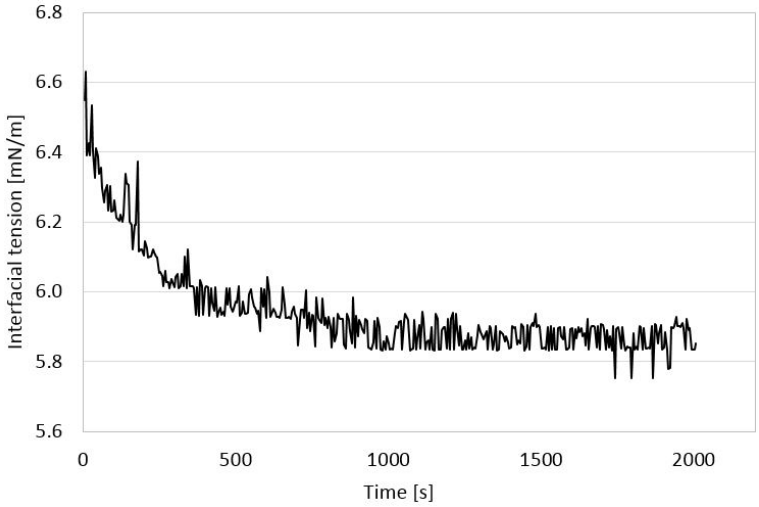

Figure 2.5: Graphical representation of IFT measurement

2.6 Contact Angle

The contact angles were measured using a goniometer of the type CAM 200 - Optical Surface Tension/Contact Angle Meter.

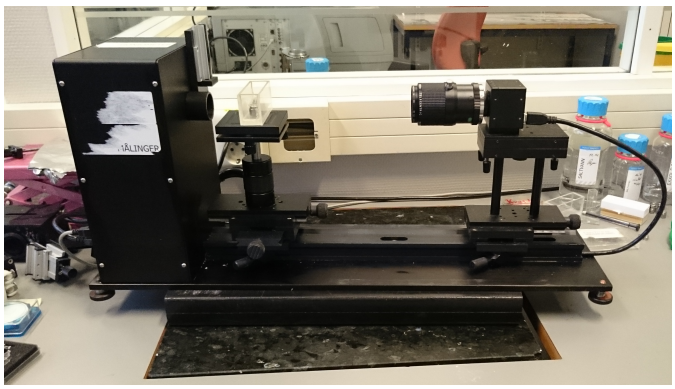

Figure 2.6: Goniometer

The following procedure is for measuring with an oil drop in water, on a glass plate. Since the density of oil is lower than density of water, the oil drop had to be placed under the glass plate.

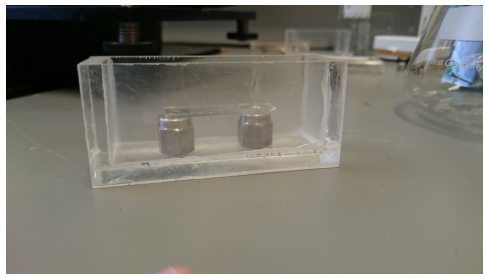

Figure 2.7: Container with glass plate and fluids

1. Select clean and dry equipment, consisting of a fluid container, a glass plate, and feet to elevate the glass plate
2. Fill container with water/nanofluid and arrange glass plate on feet inside. Make sure there are no air bubbles within the fluid.
3. Place container in front of camera, and use camera images to make sure the glass plate is level
4. Use a syringe with a hooked needle tip to place a drop of oil under the glass
5. Adjust the system so that the camera has a good view of the glass plate and the oil drop
6. Start measurement

3. Results and discussion

Nanofluid samples were first prepared with 1.0wt.% and 5.0wt.% nanoparticles, but upon trying to use the 5.0wt.% solution for measurements, it turned out to not be diluted well enough, making it possible to see suspended particles in the fluid. In figure 3.1 we see how the particles agglomerate along the rotational axis on both sides of the oil drop when trying to run an interfacial tension measurement.

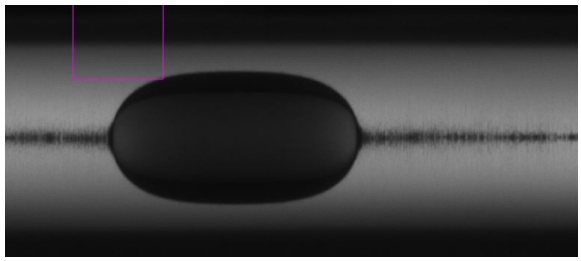

Figure 3.1: Nanoparticles agglomerating during IFT measurement

It is still possible to perform the measurement under these circumstances, but the results will not be completely reliable, in part because the actual nanofluid will have a different nanoparticle concentration than planned and in part because the particles agglomerating near the drop may interrupt the drop and change the shape, which is the basis for the calculation. In figure 3.2 we can see the nondiluted particles in the capillary tube right after stopping the interfacial tension measurement.

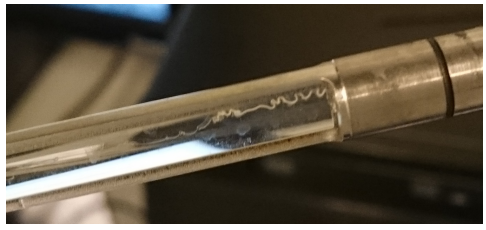

Figure 3.2: Visible nanopartcles in a capillary tube

The 5.0wt.% was replaced with 0.5wt.%, and the two nanoparticle concentrations,

as well as synthetic seawater with no nanoparticles added, were used together with the 5 oils in table 3.1 to perform the measurements described in chapter 2.

Table 3.1: Crude oil properties

Oil	Type	Density [g/ml]	Asphaltene content [%]	Wax content [%]	TAN	TBN
Gjøa Condensate	Light	0.83608	0.04	1.80	0.07	-
Grane	Asphaltic	0.94096	0.90	1.35	2.10	3.16
Norne 2	Waxy	0.87876	0.18	4.19	0.29	-
New Oseberg Blend	Paraffinic	0.83724	0.36	2.71	0.24	1.06
Troll B	Naphthenic	0.89172	0.08	1.76	1.10	1.32

3.1 Density, viscosity and refractive index

Density, viscosity and refractive index were all measured at room temperature. Table 3.2 shows the measured densities, viscosities and refractive indexes for the different nanoparticle concentrations. As we can see there is a slight increase in all three properties when adding nanoparticles, but nothing very significant.

Table 3.2: Fluid properties for the different nanoparticle concentrations

Nanoparticle concentration	Density [g/cm^3]	Viscosity [cP]	Refractive index
0.00 wt.%	1.02401	1.05290	1.3399
0.50 wt.%	1.02481	1.10568	1.3405
1.00 wt.%	1.02523	1.14860	1.3408

3.2 Interfacial Tension

The spinning drop apparatus was prepared as described in section 2.5, and run at 6000 rpm for every sample combination, with the heat set to 20°C.

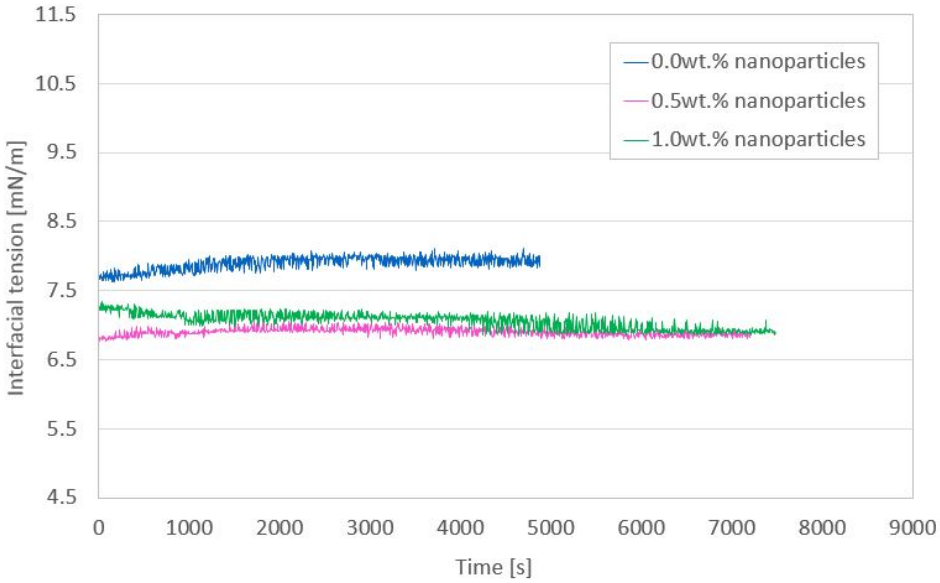

Figure 3.3: Interfacial tension for Gjøa oil

Figures 3.3 - 3.7 show the measurements of interfacial tension (IFT) over time for each oil, at the different nanoparticle concentrations. Values are approximated from these graphs where the curves even out. The time required for each measurement varies a great deal, as we can see in the figures.
In some cases, e.g. in figure 3.7 with Troll oil and no nanoparticles in the water, we see that the curve seems to even out, but later increases or decreases and then even out at a different value. This goes to show that it is possible that leaving the measurement to run longer will have caused the curve to flatten at a different value, yielding a different end result. It is, nevertheless, doubtful that such an occurrence would have made significant changes to the final results, as the case with the Troll oil only shows a change of about 0.5 mN/m and that is the most obvious one.

Table 3.3 shows the interfacial tension [mN/m] values obtained from the spinning drop measurements, and figure 3.8 shows a graphical representation of these values.

We see that the interfacial tension decreases for all five oils with the addition of nanoparticles. For the three oils from Grane, Norne and Oseberg the interfacial tension is lowest for the 0.5wt.% nanofluid. For the Gjøa oil the 0.5wt.% and 1.0wt.% nanofluids give approximately the same result and for the Troll oil the

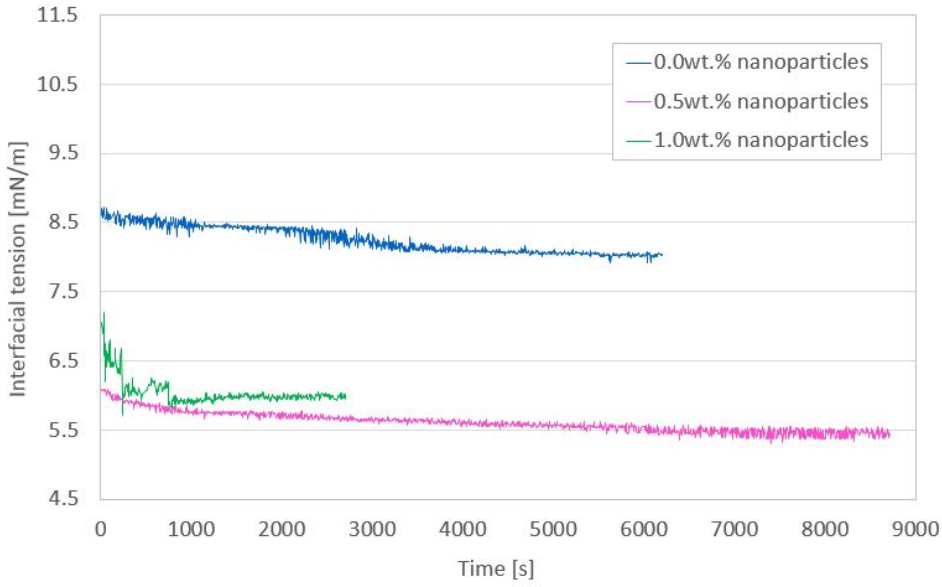

Figure 3.4: Interfacial tension for Grane oil

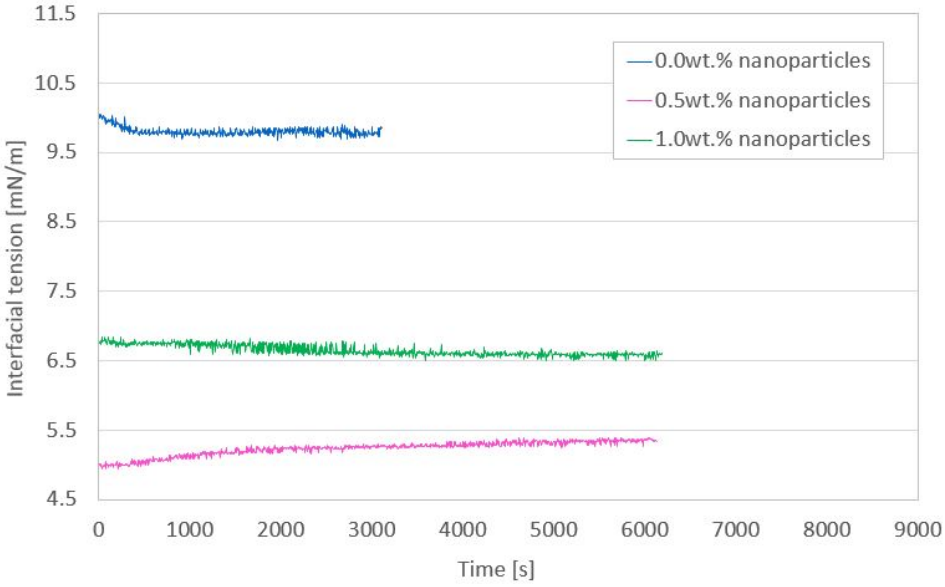

Figure 3.5: Interfacial tension for Norne oil

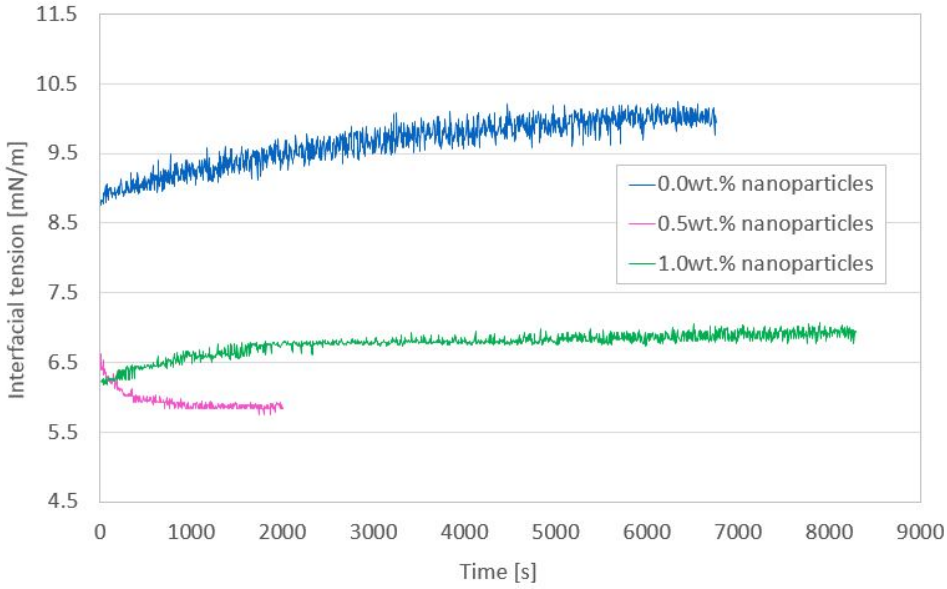

Figure 3.6: Interfacial tension for Oseberg oil

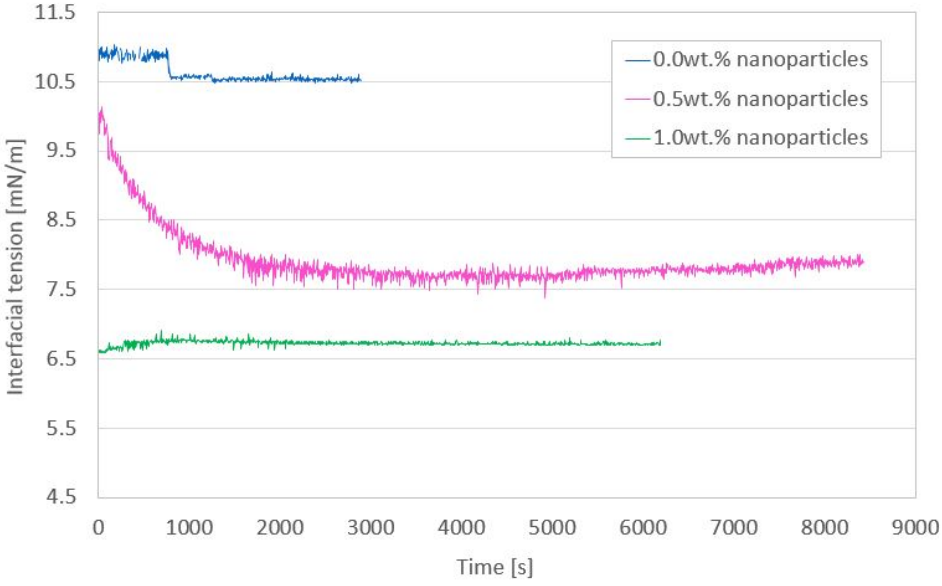

Figure 3.7: Interfacial tension for Troll oil

Table 3.3: Measured interfacial tension

Nanoparticle concentration	Oil				
	Gjøa	Grane	Norne	Oseberg	Troll
0.0 wt.%	7.93	8.03	9.77	10.01	10.53
0.5 wt.%	6.88	5.45	5.35	5.87	7.90
1.0 wt.%	6.91	5.98	6.58	6.90	6.71

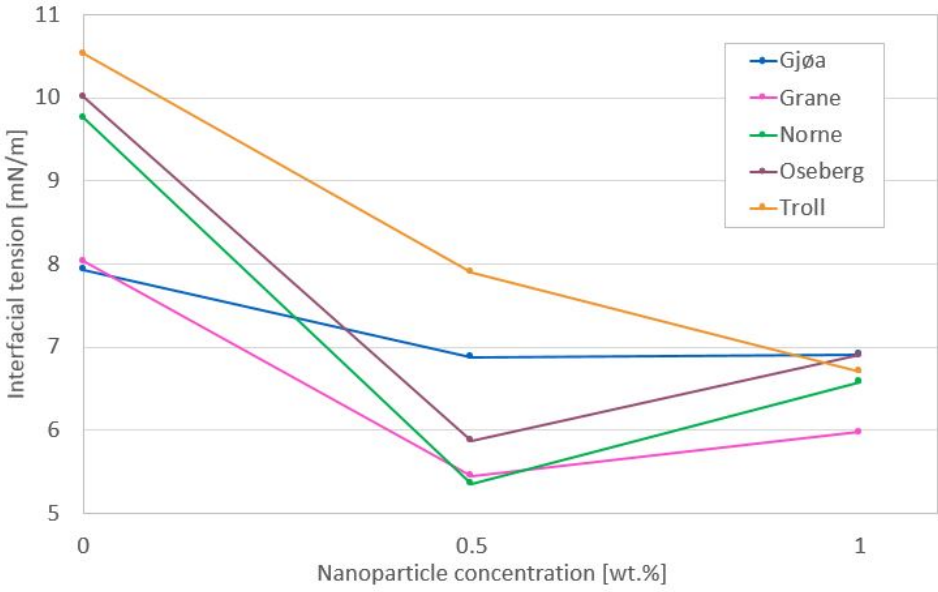

Figure 3.8: Interfacial tension vs nanoparticle concentration

1.0wt.% nanofluid give the best result.

The results vary from 7.93 mN/m to 10.53 mN/m for the brine, from 5.35 mN/m to 7.90 mN/m for the 0.5wt.% nanofluid, and from 5.98 mN/m to 6.91 mN/m for the 1.0wt.% nanofluid. This means that while the best results come from the 0.5wt.% nanofluid, all the 1.0wt.% nanofluid results fit within the range achieved for 0.5wt.% nanofluid, so even if 0.5wt.% is a better concentration for most oils, it will not be true for all oils. Also, this gives an indication that using 1.0wt.% nanoparticle concentration will give more stable, predictable results over a broad spectrum of oils. More studies will have to be done to determine the optimal nanoparticle concentration for each oil, but the results suggest that a concentration less than 1.0wt.% is preferred for most oils.

An interesting note is that the one measurement performed on the discarded 5.0wt% sample mentioned in the beginning of this chapter gave a value of approximately 6.04 mN/m, which is better than any of the other measurements with Gjøa oil. This contradicts the idea that the effects of the nanoparticles are lessened when using 1.0wt.% nanoparticles or more.

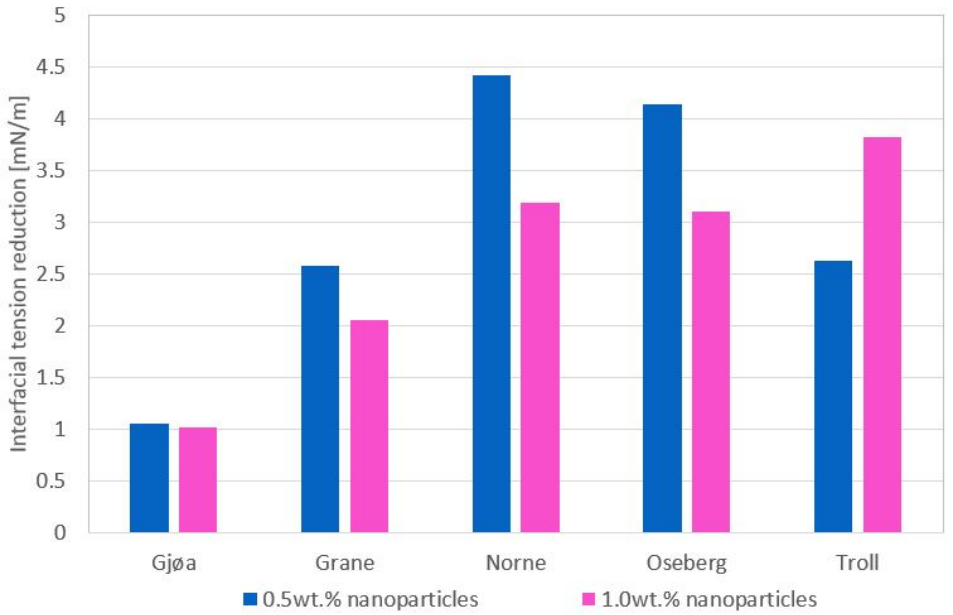

Figure 3.9: Reduction of interfacial tension

Figure 3.9 compares the reduction in interfacial tension by using 0.5wt.% and 1.0wt.% nanofluid. The biggest reduction happens for the Norne and Oseberg oils, and the least for the Gjøa oil. Gjøa has almost no difference between 0.5wt.% and 1.0wt.%, and Troll 1.0wt.% has more reduction than Gjøa and Grane for any concentration.

The use of the Funzionano nanoparticles for interfacial tension reduction shows promise, but the results from these experiments indicate that the effects are not

quite good enough. In section 1.4.1 the effect of lowering interfacial tension is discussed, and while the reduction in IFT seen in these experiments will probably have a positive effect on oil production, it is generally agreed that the IFT should be lowered at least to around 0.1 mN/m to be able to displace residual oil and to have significant effects.

3.3 Contact angle

The contact angle measurements were performed at room temperature. The software was set to take 10 pictures with 600 seconds between the pictures for all measurements, except for Norne oil with no nanoparticles in the accompanying water, which had only 400 seconds between each picture due to time constraints. The 10 pictures were each analyzed for contact angle at both the left and the right angle as seen in figure 3.10. As we can see the left and right angles are not identical, and because of this, a mean of the two are given. This mean value is the one used to obtain the following results.

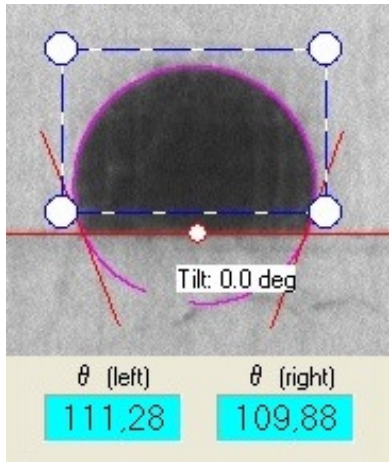

Figure 3.10: Contact angle measurement with accompanying values

The angle given by the program was the angle on the oil side, which as mentioned earlier is the opposite of the convention to measure on the side of the denser phase. The angle given by the program was subtracted from 180° so that the results follow the conventional notation, in accordance with equation 1.11.

Table 3.4: Contact angle

Nanoparticle concentration	Oil				
	Gjøa	Grane	Norne	Oseberg	Troll
0.0 wt.%	86.9	73.2	67.5	47.9	69.6
0.5 wt.%	25.8	13.4	14.3	16.5	25.8
1.0 wt.%	44.0	19.9	38.3	38.0	43.7

Table 3.4 shows the values obtained from the contact angle measurements, as an average of the 10 measurements of the mean contact angle. Figure 3.11 is a graphical representation of these values.

The graph shows a significant reduction in the contact angle, both for 0.5wt.%

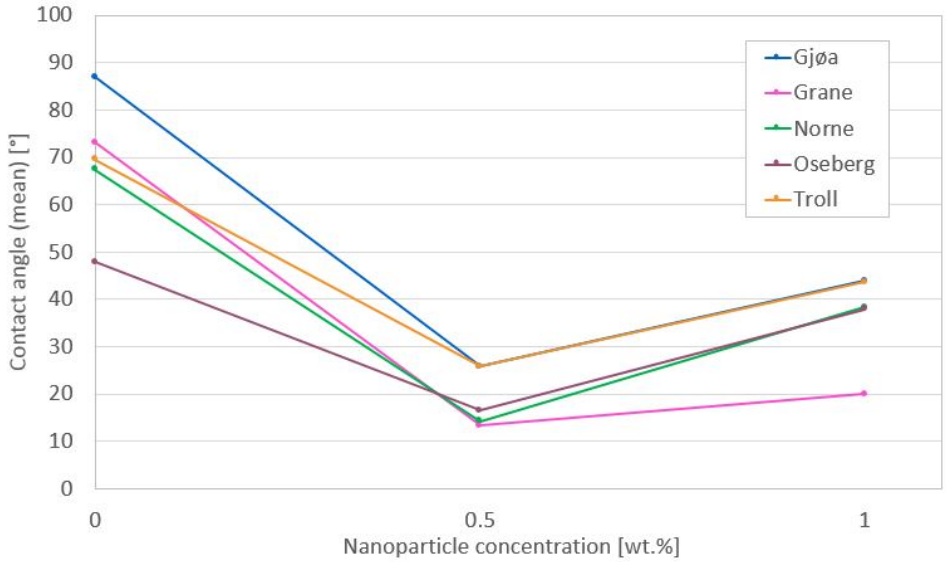

Figure 3.11: Contact angle vs nanoparticle concentration

and 1.0wt.% nanofluid, but with the best results for the 0.5wt.% for all oils. The 0.5wt.% results are better than all 1.0wt.% results with the exception of Grane where the 1.0wt.% result is the fourth best of all.

The reduction of the contact angle shows that the wetting conditions have been changed from neutral-wet to water-wet.

The contact angle results are congruent with the interfacial tension results, showing the most favorable conditions at 0.5wt.% nanofluid for most of the oils, and again the best results are for the Grane, Norne and Oseberg oils.

Figure 3.12 compares the reduction in contact angle by using 0.5wt.% and 1.0wt.% nanoparticle concentration. The angle is reduced most for Gjøa and Grane and least for Oseberg, both for 1.0wt.% and 0.5wt.%. This is opposite of the IFT results where the nanoparticles influenced Norne and Oseberg most and had the smallest effect on Gjøa and Grane.

Table 3.5: Reduction of interfacial tension and contact angle

Nanoparticle concentration	Interfacial tension [mN/m]		Contact angle [°]	
	Average reduction	Maximum reduction	Average reduction	Maximum reduction
0.5 wt.%	2.96	4.14	49.9	61.2
1.0 wt.%	2.64	3.82	32.2	53.3

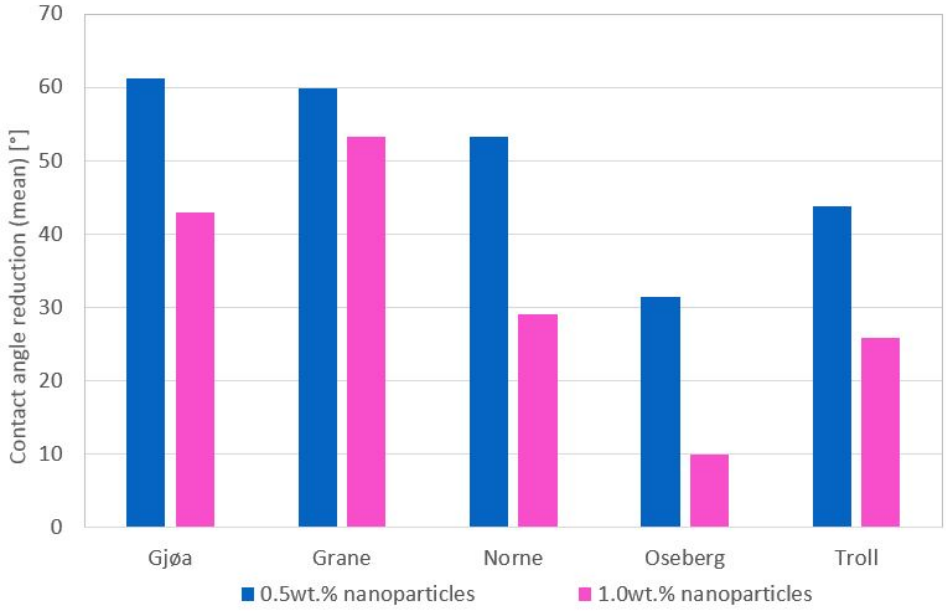

Figure 3.12: Reduction of contact angle

Table 3.5 show the average and maximum reductions of interfacial tension and contact angle by addition of 0.5wt.% and 1.0wt.% nanoparticles. For interfacial tension the maximum result for 0.5wt.% and 1.0wt.% is from Norne and Troll respectively. For contact angle the maximum result for 0.5wt.% and 1.0wt.% is from Gjøa and Grane respectively.

3.4 Sources of error

A new table of oil properties were provided after all measurements were finished, where the oil densities of the Gjøa and Grane oils were slightly altered. The density of the oils have been used in the software that calculates the results, and this may have had an effect on the final results. Some of the other properties were altered as well, but they were not used in any calculations so only the new values for these are given.

Table 3.6: New densities

Oil	Old density [g/ml]	New density [g/ml]
Gjøa Condensate	0.83608	0.83091
Grane	0.94096	0.94153
Norne 2	0.87876	0.87876
New Oseberg Blend	0.83724	0.83724
Troll B	0.89172	0.89172

There has been some speculation about whether the SVT 20 that was used is properly calibrated and whether it gives results that are not correct, due to a few people experiencing getting unexpected results. This issue was not sorted by the time the measurements were finished. The results obtained should still be comparable to each other, but may not be comparable to other studies.

Due to difficulty in making the oil drops for both the interfacial tension and contact angle measurement, the drop sizes varied somewhat. There has not been any obvious consequences of this, but it may have caused the measurements to be slightly different than they would have been with identically sized oil drops.

3.5 Suggestions for future work

There is still much work that can be done to get a complete overview of how the Funzionano nanoparticles effect fluid properties.

The measurements can be performed:

- with other nanoparticle concentrations
- at different temperatures
- at different pressures
- with other oils
- using other measurement techniques

The Funzionano nanoparticles show potential, and it may very well be worth looking more into how they interact with different fluids.

4. Conclusion

The addition of nanoparticles to this specific synthetic saltwater shows promise when it comes to reducing interfacial tension and contact angle. Overall, the results with 0.5wt.% added nanoparticles are better than the results with 1.0wt.% added nanoparticles.

Unfortunately, the interfacial tension results are not as good as hoped, but it is possible that with further testing an optimal concentration will be found that gives better results. The wettability alteration is good, but may not give equally good results for other solid surfaces that are more likely to be seen in a reservoir.

Bibliography

James Sheng. *Modern chemical enhanced oil recovery theory and practice*. Gulf Professional Pub., Amsterdam; Boston, 2011. ISBN 9780080961637 0080961630 1856177459 9781856177450. URL http://www.books24x7.com/marc.asp?bookid=40119.

Ole Torsæter. Class Presentation: TPG 4112 Geomekanikk og strømning i porøse media, Del 2: Strømning i porøse media, Noen slides om metning og kapillærtrykk, March 2011a.

"Steamflood". URL http://www.glossary.oilfield.slb.com/en/Terms.aspx?LookIn=term%20name&filter=steamflood.

"In-situ combustion". URL http://petrowiki.org/In-situ_combustion.

"API Background Report". Summary of Carbon Dioxide Enhanced Oil Recovery (CO2eor) Injection Well Technology. URL http://www.api.org/~/media/files/ehs/climate-change/summary-carbon-dioxide-enhanced-oil-recovery-well-tech.pdf.

"Density, Specific Weight and Specific Gravity". URL http://www.engineeringtoolbox.com/density-specific-weight-gravity-d_290.html.

"Dynamic, Absolute and Kinematic Viscosity". URL http://www.engineeringtoolbox.com/dynamic-absolute-kinematic-viscosity-d_412.html.

Duncan J. Shaw. *Introduction to colloid and surface chemistry*. Butterworth-Heinemann, Oxford ; Boston, 4th ed edition, 1992. ISBN 0750611820.

Souheng Wu. Calculation of interfacial tension in polymer systems. *Journal of Polymer Science Part C: Polymer Symposia*, 34(1):19–30, 1971. ISSN 04492994, 19353065. doi: 10.1002/polc.5070340105. URL http://doi.wiley.com/10.1002/polc.5070340105.

Wael Abdallah, Jill S. Buckley, Andrew Carnegie, John Edwards, Edmund Fordham, Arne Graue, Tarek Habashy, Bernd Herold, Nikita Seleznev, Claude Signer, Hassain Hussain, Bernard Montaron, and Murtaza Ziauddin. Fundamentals of Wettability. *Oilfield Review*, 19(2), June 2007. URL http://www.slb.com/~/media/Files/resources/oilfield_review/ors07/sum07/p44_61.aspx.

Martin J. Blunt. Constraints on Contact Angles for Multiple Phases in Thermodynamic Equilibrium. *Journal of Colloid and Interface Science*, 239(1):281–282, July 2001. ISSN 00219797. doi: 10.1006/jcis.2001.7534. URL http://linkinghub.elsevier.com/retrieve/pii/S0021979701975344.

"Relative permeability and capillary pressure", September 2013. URL http://petrowiki.org/Relative_permeability_and_capillary_pressure.

Ole Torsæter. Class Presentation: TPG 4112 Geomekanikk og strømning i porøse media, Del 2: Strømning i porøse media, Relativ permeabilitet, March 2011b.

Jude O. Amaefule and Lyman L. Handy. The Effect of Interfacial Tensions on Relative Oil/Water Permeabilities of Consolidated Porous Media. *Society of Petroleum Engineers Journal*, 22(03):371–381, June 1982. ISSN 0197-7520. doi: 10.2118/9783-PA. URL http://www.onepetro.org/doi/10.2118/9783-PA.

M.C. Leverett. Flow of Oil-water Mixtures through Unconsolidated Sands. *Transactions of the AIME*, 132(01):149–171, December 1939. ISSN 0081-1696. doi: 10.2118/939149-G. URL http://www.onepetro.org/doi/10.2118/939149-G.

D.G. Longeron. Influence of Very Low Interfacial Tensions on Relative Permeability. *Society of Petroleum Engineers Journal*, 20(05):391–401, October 1980. ISSN 0197-7520. doi: 10.2118/7609-PA. URL http://www.onepetro.org/doi/10.2118/7609-PA.

E.C. Donaldson, G.V. Chilingarian, and T.F. Yen. *Enhanced Oil Recovery, II: Processes and Operations*. Elsevier, 1989.

O.R. Wagner and R.O. Leach. Effect of Interfacial Tension on Displacement Efficiency. *Society of Petroleum Engineers Journal*, 6(04):335–344, December 1966. ISSN 0197-7520. doi: 10.2118/1564-PA. URL http://www.onepetro.org/doi/10.2118/1564-PA.

W.W. Owens and D.L. Archer. The Effect of Rock Wettability on Oil-Water Relative Permeability Relationships. *Journal of Petroleum Technology*, 23(07):873–878, July 1971. ISSN 0149-2136. doi: 10.2118/3034-PA. URL http://www.onepetro.org/doi/10.2118/3034-PA.

IUPAC. Terminology for biorelated polymers and applications (IUPAC Recommendations 2012)*, 2012. URL http://pac.iupac.org/publications/pac/pdf/2012/pdf/8402x0377.pdf.

"What's So Special about the Nanoscale?". URL http://www.nano.gov/nanotech-101/special.

Martin Vad Bennetzen and Kristian Mogensen. Novel Applications of Nanoparticles for Future Enhanced Oil Recovery. International Petroleum Technology Conference, 2014. doi: 10.2523/17857-MS. URL http://www.onepetro.org/doi/10.2523/17857-MS.

Jihua Cai, Martin E. Chenevert, Mukul M. Sharma, and James E. Friedheim. Decreasing Water Invasion Into Atoka Shale Using Nonmodified Silica Nanoparticles. *SPE Drilling & Completion*, 27(01):103–112, March 2012. ISSN 1064-

6671. doi: 10.2118/146979-PA. URL http://www.onepetro.org/doi/10.2118/146979-PA.

Taner Sensoy, Martin E. Chenevert, and Mukul Mani Sharma. Minimizing Water Invasion in Shales Using Nanoparticles. Society of Petroleum Engineers, 2009. doi: 10.2118/124429-MS. URL http://www.onepetro.org/doi/10.2118/124429-MS.

Tianping Huang, James B. Crews, and John Robert Willingham. Using Nanoparticle Technology to Control Fine Migration. Society of Petroleum Engineers, 2008. doi: 10.2118/115384-MS. URL http://www.onepetro.org/doi/10.2118/115384-MS.

N.A. Ogolo, O.A. Olafuyi, and M.O. Onyekonwu. Enhanced Oil Recovery Using Nanoparticles. Society of Petroleum Engineers, 2012. doi: 10.2118/160847-MS. URL http://www.onepetro.org/doi/10.2118/160847-MS.

Shidong Li, Luky Hendraningrat, and Ole Torsaeter. Improved Oil Recovery by Hydrophilic Silica Nanoparticles Suspension: 2-Phase Flow Experimental Studies. International Petroleum Technology Conference, 2013. doi: 10.2523/16707-MS. URL http://www.onepetro.org/doi/10.2523/16707-MS.

Abbas Roustaei, Jamshid Moghadasi, Hadi Bagherzadeh, and Abbas Shahrabadi. An Experimental Investigation of Polysilicon Nanoparticles' Recovery Efficiencies through Changes in Interfacial Tension and Wettability Alteration. Society of Petroleum Engineers, 2012. doi: 10.2118/156976-MS. URL http://www.onepetro.org/doi/10.2118/156976-MS.

Ali Karimi, Zahra Fakhroueian, Alireza Bahramian, Nahid Pour Khiabani, Jabar Babaee Darabad, Reza Azin, and Sharareh Arya. Wettability Alteration in Carbonates using Zirconium Oxide Nanofluids: EOR Implications. *Energy & Fuels*, 26(2):1028–1036, February 2012. ISSN 0887-0624, 1520-5029. doi: 10.1021/ef201475u. URL http://pubs.acs.org/doi/abs/10.1021/ef201475u.

Fawaz Mohammed Al Otaibi, Sunil Lalchand Kokal, Yun Chang, Jassi F. AlQahtani, and Amin M. AlAbdulwahab. Gelled Emulsion of CO-Water-Nanoparticles. Society of Petroleum Engineers, 2013. doi: 10.2118/166072-MS. URL http://www.onepetro.org/doi/10.2118/166072-MS.

Shahab Ayatollahi and Mohammad M. Zerafat. Nanotechnology-Assisted EOR Techniques: New Solutions to Old Challenges. Society of Petroleum Engineers, 2012. doi: 10.2118/157094-MS. URL http://www.onepetro.org/doi/10.2118/157094-MS.

Ali Elsaeh Enbaia and Illiya Amalina Binti Ahmad Ramdzani. Pore size and geometry of reservoir rocks used as key factor for drilling and completion fluid design of oil wells. *European Scientific Journal*, 10(10), 2014. URL http://www.eujournal.org/index.php/esj/article/view/3263.

Nicolas Rival. FunzioNano, January 2015.

Elda Markovic, Kristina Constantopolous, and Janis G. Matisons. Polyhedral Oligomeric Silsesquioxanes: From Early and Strategic Development through

to Materials Application. In Claire Hartmann-Thompson, editor, *Applications of Polyhedral Oligomeric Silsesquioxanes*, volume 3, pages 1–46. Springer Netherlands, Dordrecht, 2011. ISBN 978-90-481-3786-2, 978-90-481-3787-9. URL http://www.springerlink.com/index/10.1007/978-90-481-3787-9_1.

"Artificial seawater". URL http://en.wikipedia.org/wiki/Artificial_seawater.

Dana R. Kester, Iver W. Duedall, Donald N. Connors, and Ricardo M. Pytkowicz. Preparation of Artificial Seawater, 1967. URL http://aslo.org/lo/toc/vol_12/issue_1/0176.pdf.

O Torsæter and M Abtahi. Experimental reservoir engineering laboratory workbook, 2003.

DataPhysics. Application note 23. Determination of low interfacial tensions with DataPhysics Spinning Drop Tensiometer SVT 20n.

Appendices

A. Drop Images from interfacial tension and contact angle measurements

Drop images from interfacial tension measurement

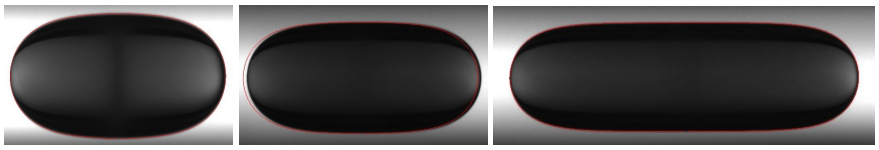

(a) Brine (b) 0.5wt.% (c) 1.0wt.%

Figure A.1: Gjøa IFT drops

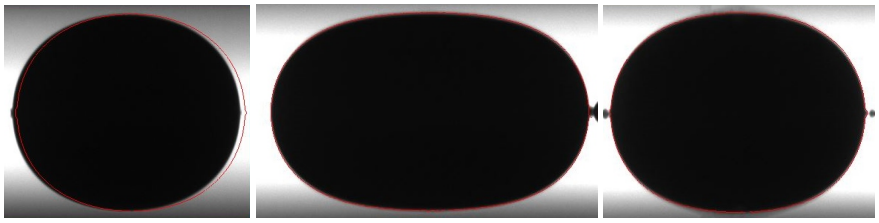

(a) Brine (b) 0.5wt.% (c) 1.0wt.%

Figure A.2: Grane IFT drops

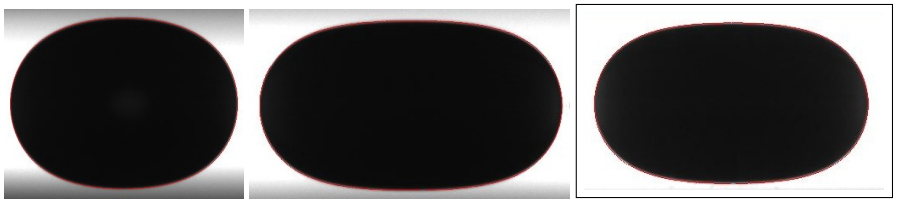

(a) Brine (b) 0.5wt.% (c) 1.0wt.%

Figure A.3: Norne IFT drops

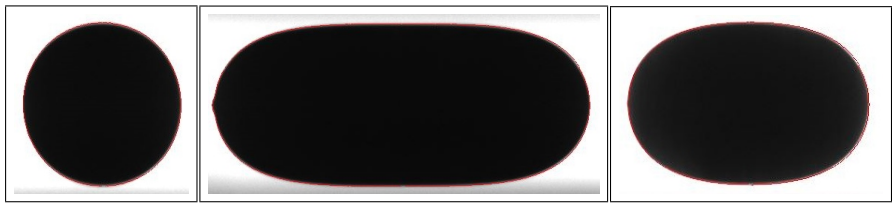

(a) Brine (b) 0.5wt.% (c) 1.0wt.%

Figure A.4: Oseberg IFT drops

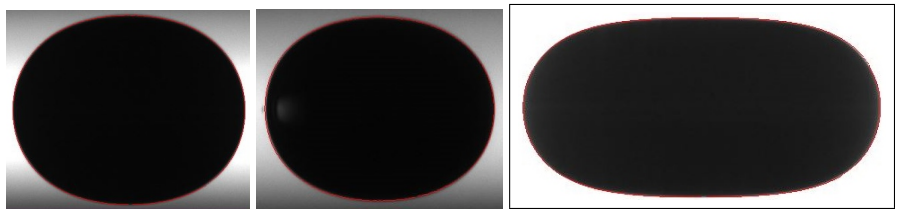

(a) Brine (b) 0.5wt.% (c) 1.0wt.%

Figure A.5: Troll IFT drops

Drop images from contact angle measurement

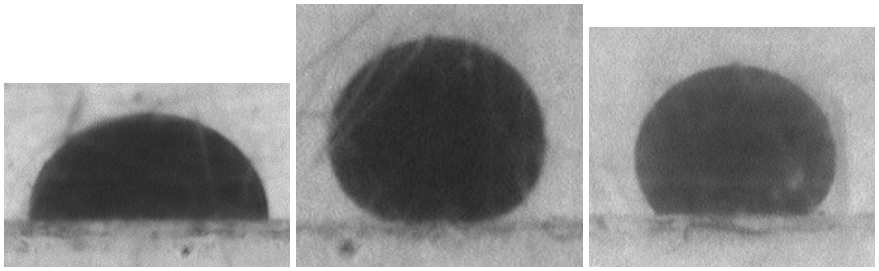

(a) Brine (b) 0.5wt.% (c) 1.0wt.%

Figure A.6: Gjøa contact angle drops

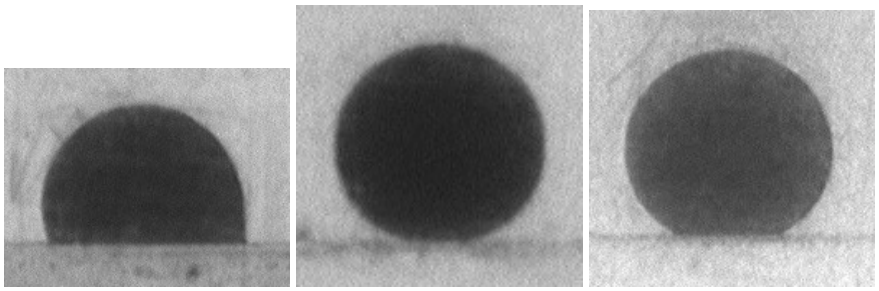

(a) Brine (b) 0.5wt.% (c) 1.0wt.%

Figure A.7: Grane contact angle drops

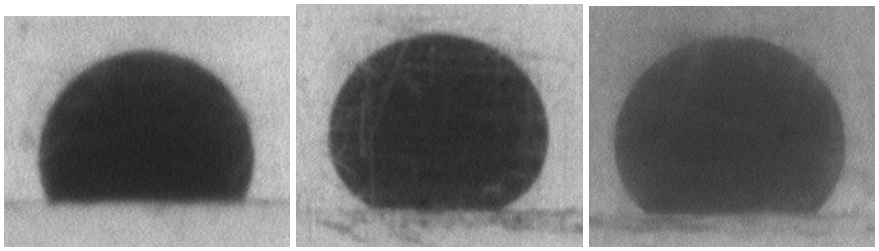

(a) Brine (b) 0.5wt.% (c) 1.0wt.%

Figure A.8: Norne contact angle drops

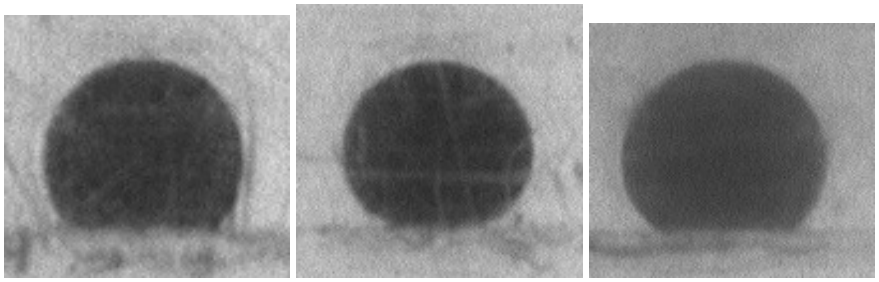

(a) Brine (b) 0.5wt.% (c) 1.0wt.%

Figure A.9: Oseberg contact angle drops

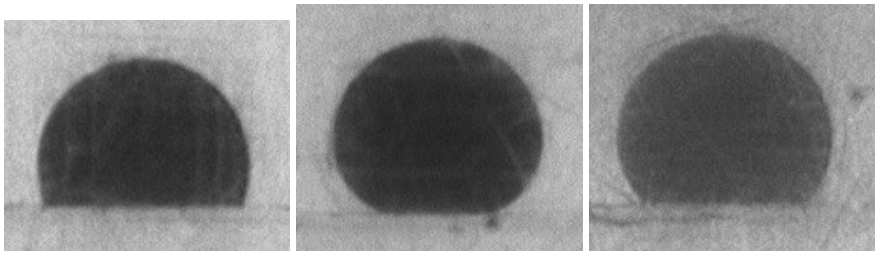

(a) Brine (b) 0.5wt.% (c) 1.0wt.%

Figure A.10: Troll contact angle drops